Journal of Colloid and Interface Science 415 (2014) 151–158

Contents lists available at ScienceDirect

Journal of Colloid and Interface Science

www.elsevier.com/locate/jcis

Effects of crosslinker on the morphology and properties of microgels containing *N*-vinylformamide, glycidylmethacrylate and vinylamine

Judith McCann [a], Sineenat Thaiboonrod [a], Rein V. Ulijn [b], Brian R. Saunders [a,*]

[a] Biomaterials Research Group, Manchester Materials Science Centre, School of Materials, The University of Manchester, Grosvenor Street, Manchester M1 7HS, UK
[b] Department of Pure and Applied Chemistry/WestCHEM, University of Strathclyde, Cathedral Street, Glasgow G1 1XL, UK

ARTICLE INFO

Article history:
Received 5 August 2013
Accepted 12 September 2013
Available online 21 September 2013

Keywords:
Microgel
N-vinylformamide
Vinylamine
Glycidylmethacrylate
Polymer particles
Polyampholyte

ABSTRACT

Microgels are swollen crosslinked polymer colloid particles. We used non-aqueous dispersion polymerisation to prepare new water-swellable microgels containing *N*-vinylformamide (NVF), glycidylmethacrylate (GMA) and an alkali-stable crosslinker, 2-(*N*-vinylformamido)ethyl ether (NVE). The microgel particles had a core that was rich in NVF. The shell contained GMA and NVF. In order to expose the amine functionality, alkaline hydrolysis was used, transforming the NVF groups in the shell to vinylamine (VAM) while leaving most NVF in the core untouched. The hydrolysed microgels (H-NVF–GMA–NVE) were cationic at low pH and were shown to have polyampholyte behaviour. Inclusion of NVE had the beneficial effects of preventing microphase separation at the microgel surface and stabilising the polyampholyte structure against excessive fragmentation during hydrolysis. These new water-swellable core–shell microgels were prepared using scalable methods and may enable future preparation of functionalised core–shell microgels and composites.

1. Introduction

Microgels are crosslinked polymer particles that swell in a good solvent [1–7]. Core–shell microgels have attracted special interest because they provide opportunities for constructing particles with controlled nanometre scale architecture and interesting properties [8–10]. Unfortunately, there is a lack of water-swellable microgel types available. The overwhelming majority of microgel research has involved poly(*N*-isopropylacrylamide), PNP [1,4,7]. Moreover, there are few examples of water-swellable cationic microgels that do not contain PNP. Two non-PNP microgel types that have been widely studied are pH-responsive microgels based on methacrylic acid [11,12] or 2-vinylpyridine [13]. We recently demonstrated that non-aqueous dispersion polymerisation (NAD) could be used to prepare microgels based on *N*-vinylformamide (NVF) [14,15]. Copolymerisation of NVF with glycidylmethacrylate (GMA) produced NVF–GMA microgels with a non-uniform "cane-ball" morphology [15]. In that study it was shown that GMA provided a source of crosslinking which was proposed to occur via a NVF–GMF reaction [15]. Alkali hydrolysis is well known to convert NVF segments to vinylamine (VAM) [16,17] and was used in those studies [14,15]. PVAM has the highest primary amine content of all known amine-containing polymers and is structurally similar to polyethyleneimine (PEI). Polymers [17] and microgels [14] containing primary amines offer excellent potential for functionalization. There are relatively few examples of PVAM microgels and most of those involve copolymerisation with NP [14,18–20]. Here, we extend our earlier investigation of core–shell cane-ball PNVF–GMA microgels [15] by incorporating a recently established crosslinker [21], 2-(*N*-vinylformamido)ethyl ether (NVE), into these microgels for the first time. We demonstrate that inclusion of NVE provides a uniform morphology and reduced particle fragmentation during the alkaline hydrolysis step used to expose the primary amines and by doing so improves the structural stability of the hydrolysed microgels, which are polyampholytes.

Polymer colloids which contain VAM as the primary component have been mostly studied in hollow particle form. Kim et al. used a sacrificial crosslinker (*N*, *N*'-methylene bisacrylamde, BA) and a diffusion-limited reaction to prepare hollow VAM particles from NVF particles [22]. In an elegant colloidal template approach, Berkland and Shi used silica particles to construct a crosslinked NVF shell, which was then hydrolysed to VAM [23]. Alkaline hydrolysis simultaneously hydrolysed NVF to VAM and removed the silica core. In the following we explore a scalable approach to prepare core–shell microgels with a shell containing VAM. Compared to hollow particles, core–shell microgels offer higher overall particle

* Corresponding author. Address: Biomaterials Research Group, School of Materials, Grosvenor Street, Manchester M13 9PL, UK. Fax: +44 161 306 3586.
E-mail addresses: judith.mccann@postgrad.manchester.ac.uk (J. McCann), sineenat.thaiboonrod@postgrad.manchester.ac.uk (S. Thaiboonrod), rein.ulijn@strath.ac.uk (R.V. Ulijn), brian.saunders@manchester.ac.uk (B.R. Saunders).

0021-9797
http://dx.doi.org/10.1016/j.jcis.2013.09.030

modulus for potential engineering applications and have many additional functionalization potential within the core.

NVE (See Scheme 1) is a new crosslinking monomer that was established to retain its crosslinking segments after alkaline hydrolysis [21,24]. Traditional crosslinking monomers such as BA are cleaved during alkaline hydrolysis [22] and are not suitable for VAM microgel preparation. We recently used NVE to successfully prepare NVF–NVE microgels which were successfully hydrolysed to high primary amine content VAM microgels [14]. Here, we investigate core–shell microgels prepared by copolymerisation of GMA, NVF and NVE for the first time. The microgels are termed NVF_x–GMA_y–NVE_z, where x, y and z are the mole fractions of NVF, GMA and NVE used during preparation. The non-hydrolysed NVF_x–GMA_y–NVE_z latexes were prepared by NAD (Scheme 1). They were then redispersed in water to give (non-hydrolysed) NVF_x–GMA_y–NVE_z microgels. The dispersions were then subjected to alkaline hydrolysis to transform NVF into VAM. The hydrolysed microgels are termed H-NVF_x–GMA_y–NVE_z because hydrolysis was not complete. Two hypotheses investigated in this study are that inclusion of a crosslinking monomer (NVE) should restrict microphase separation previously observed within NVF–GMA microgels [15] and also its inclusion should reduce particle fragmentation during hydrolysis.

The novelty of the present study originates from the new microgels which contained NVF, GMA and NVE. Our previous work involved microgels containing only two of these monomers, i.e., NVF–GMA [15] or NVF–NVE [14]. The new NVF_x–GMA_y–NVE_z and H-NVF_x–GMA_y–NVE_z microgels studied here have different morphologies, properties and stability to alkaline hydrolysis compared to the earlier systems [14,15]. New findings from this study are reported regarding the role of crosslinking monomer on microgel particle morphology and polyampholyte stability to fragmentation as well as the origin of the ability of added GMA to decrease NVF hydrolysis efficiency. Because the microgels had improved stability and contained accessible epoxide or amine groups, which are well-suited to functionalization [14,25], they may have potential for application in areas such as biomaterials [26], surface coatings [27] and hybrid microgel/nanoparticle composites [28].

2. Materials and methods

2.1. Materials

GMA, (97%), NVF (98%), isopropanol (IPA, 99.5%), azobisobutyronitrile (AIBN, 98%), poly(vinylpyrrolidone) (PVP, $M_n \sim 40{,}000$) and ethanol (GPR grade) were purchased from Aldrich and used as received. Sodium fluorescein was also purchased from Aldrich and used as received. NVE was prepared and characterised using the method described in detail earlier [14].

2.2. Preparation of dispersions of microgels containing NVF

All of the NVF_x–GMA_y–NVE_z microgels were prepared using similar procedures. An example preparation is described in the following for NVF_{63}–GMA_{32}–NVE_5. In this case, NVF (4.0 g, 0.0563 mol), GMA (4.0 g, 0.028 mol) and NVE (1.0 g, 0.00472 mol) were added at a uniform rate to a pre-purged 250 ml four-necked round bottomed flask containing IPA (68 ml), PVP (1.8 g) and AIBN (0.241 g, 0.00147 mol). The flask was equipped with a mechanical stirrer, condenser, feed tube and nitrogen gas inlet. The feed commenced at a temperature of 80 °C and was conducted over 1 h. The reaction was allowed to continue for a further 6 h under moderate stirring. The product was purified by repeated centrifugation and redispersion in ethanol. IPA and ethanol are non-solvents for PNVF. Here, the NVF_{66}–GMA_{34} was prepared and purified using an equivalent method to that described above. The quantities of monomer used for each preparation appear in Table 1.

2.3. Preparation of microgels containing VAM

Non-hydrolysed NVF_x–GMA_y–NVE_z microgel particles (1 g) were obtained by centrifugation and redispersed in 4 ml of ethanol. The dispersion was added dropwise to 100 ml of aqueous 1 M NaOH solution which was stirred and heated to 80 °C. The hydrolysis reaction was continued for a further 18 h. The dispersion was then washed twice in 0.01 M NaOH (using centrifugation and redispersion) and then the pH was lowered to about 3.0 using 0.01 M HCl solution, The microgel particles were then centrifuged once more and redispersed in water at pH = 3.0.

2.4. Physical measurements

Optical microscopy was conducted with an Olympus BX41 microscope. Zeta potentials (ζ) and hydrodynamic diameters (d_h) were measured using a Malvern Zetasizer. The ζ values were calculated from the electrophoretic mobilities using the Smoluchowski equation [29]. A background electrolyte concentration of 0.001 M $NaNO_3$ was used for the ζ measurements. The microgel particle volume swelling ratio (Q) was estimated from the ratio of the swollen microgel particle volume to the collapsed particle volume determined from dynamic light scattering (DLS) measurements. The equation used was $Q = (d_h/d_{h(c)})^3$, where d_h and $d_{h(c)}$ are the hydrodynamic diameters measured in water and ethanol, respectively. The $d_{h(c)}$ values were measured using the parent non-hydrolysed latex (collapsed) form of the particles. SEM measurements were obtained using a Philips FEGSEM instrument. The samples

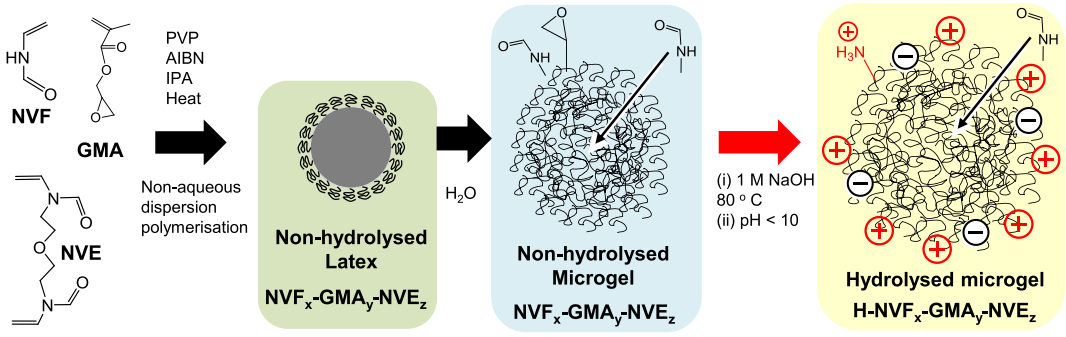

Scheme 1. Preparation of latex and microgels containing NVF, GMA and NVE. The particles were first prepared in latex form and then redispersed in water to give a non-hydrolysed microgel. Reaction with aqueous NaOH solution produced hydrolysed microgels which displayed polyampholyte behaviours.

Table 1
Compositions used to prepare the non-hydrolysed NVE_x–GMA_y–NVE_z latexes.

Code	y[a]	NVF (g)	GMA (g)	NVE (g)	%N/%C calc for y	%N/%C found
NVF_{66}–GMA_{34}	0.34	4.5	4.5	0	0.180	0.170
NVF_{63}–GMA_{32}–NVE_5	0.32	4.0	4.0	1.0	0.185	0.175
NVF_{73}–GMA_{22}–NVE_5	0.22	5.0	3.0	1.0	0.230	0.230
NVF_{81}–GMA_{14}–NVE_5	0.14	6.0	2.0	1.0	0.275	0.265

[a] Mole fraction of GMA used during preparation.

were dried at room temperature and coated with carbon. At least 60 particles were measured to determine the number-average diameters (D_{SEM}). Fourier transform infrared (FTIR) measurements were conducted using a Nicolet 5700 FTIR spectrometer.

2.5. Confocal microscopy measurements

Confocal microscopy was performed using a Leica TCS SP5 broadband confocal microscope. The excitation and emission wavelengths were 460 and 515 nm, respectively. Labelling of H-NVF_{73}–GMA_{22}–NVE_5 was performed using sodium fluorescein in the following manner. H-NVF_{73}–GMA_{22}–NVE_5 dispersion (0.5 ml, 0.15 wt.%) was added to 3 ml of pH = 5.8 buffer. Then the chromophore (1 wt.% in water with respect to the microgel particles) was added and the dispersion mixed end-over-end for 24 h. The dispersion was subsequently washed extensively with buffer solution using centrifugation and redispersion to remove excess chromophore.

3. Results and discussion

In this work three new microgels were prepared and studied. We use the abbreviation (H-)NVF_x–GMA_y–NVE_z to refer to both hydrolysed and non-hydrolysed microgels collectively. They were prepared using different y values (Table 1). (H-)NVF_{66}–GMA_{34} was used as a model system and it provided insight into the effects of added NVE on (H-)NVF_x–GMA_y–NVE_z morphology, composition and properties.

3.1. Composition changes of NVF_x–GMA_y–NVE_z microgels due to hydrolysis

The elemental analysis data shown in Table 1 support the view that the conversions of the monomers to polymer were high because there was good agreement between the calculated and found %N/%C ratios. From our previous studies on related NVF–GMA and NVF–NVE microgels it was established that the %N/%C ratio from elemental analysis was a useful parameter to assess the extent of alkaline hydrolysis and microgel fragmentation [14,15]. The coefficient of variation for the %N/%C values was less than 0.3% based on repeat measurements of related materials to those studied in this work. Fig. 1 shows a plot of the %N/%C values for both the non-hydrolysed NVF_x–GMA_y–NVE_z particles and also the hydrolysed H-NVF_x–GMA_y–NVE_z particles as a function of the GMA mole fraction (y) used to prepare the NVF_x–GMA_y–NVE_z particles. The figure also shows the key region of the FTIR spectra for each (H-)NVF_x–GMA_y–NVE_z system. Wider wavenumber range FTIR spectra for each system are shown in Fig. S1. Based on work on related NVF–GMA systems [15], a %N/%C ratio for H-NVF_x–GMA_y–NVE_z that is less than the value of the non-hydrolysed NVF_x–GMA_y–NVE_z precursor is an indication of hydrolysed polymer loss from the microgel particles. It can be inferred from Fig. 1 that significant particle fragmentation occurred (%N/%C decreased) at the two composition extremes, i.e., for low the systems containing low GMA (H-NVF_{81}–GMA_{14}–NVE_5) or no NVE (H-NVF_{66}–GMA_{34}). For the two intermediate compositions (H-NVF_{73}–GMA_{22}–NVE_5 and H-NVF_{63}–GMA_{32}–NVE_5) there was no significant change of the %N/%C ratios as a result of hydrolysis. For these two systems this means either that there no (or minimal) hydrolysis occurred or there was less hydrolysed polymer loss due to fragmentation from the microgels compared to H-NVF_{81}–GMA_{14}–NVE_5 and H-NVF_{66}–GMA_{34}. The FTIR spectra and zeta potential data (below) show that significant hydrolysis occurred for each system, pointing to less fragmentation (and increased microgel structural stability) for H-NVF_{73}–GMA_{22}–NVE_5 and H-NVF_{63}–GMA_{32}–NVE_5 during hydrolysis.

The FTIR spectra for the (non-hydrolysed) NVF_x–GMA_y–NVE_z latex particles (dotted lines in the spectra shown in Fig. 1) showed amide I and II bands in the regions of 1655 and 1530 cm^{-1}, respectively. Whilst the former band is attributed to predominantly amide C═O stretching, the latter is due to N—H bending [30]. The spectra for NVF_x–GMA_y–NVE_z also showed the presence of carbonyl groups due to the ester linkage (1725 cm^{-1}) of GMA and the band intensity increased with y. Another trend for NVF_x–GMA_y–NVE_z that can be seen from the wider range spectra (Fig. S1) is that the relative intensity of the epoxide group band (907 cm^{-1}) increased with y confirming GMA incorporation. A significant proportion of the epoxide groups were unreacted after NVF_x–GMA_y–NVE_z particle formation. Hence, they were available for subsequent reaction.

The spectra for the H-NVF_x–GMA_y–NVE_z microgels (solid lines in Fig. 1) retained the dominant amide I and amide II bands. Accordingly, hydrolysis of the NVF segments to VAM was not complete and the hydrolysed microgels contained mostly NVF segments. (Fig. 5(a) shows that a major increase in ζ occurred which means that VAM was produced.) It is remarkable that inclusion of relatively small proportions of GMA (e.g., 14 mol.% for H-NVF_{81}–GMA_{14}–NVE_5) greatly decreased NVF hydrolysis efficiency. This is despite the fact that the conditions used for hydrolysis were those that caused almost complete conversion of NVF–NVE to VAM microgels in previous work [14]. This confirms a trend established for NVF–GMA microgels earlier [15]. We return to this subject later.

Closer inspection of the spectra in Fig. 1 show that there was considerable broadening of the spectra in the 1600 cm^{-1} region. Indeed for the low GMA (H-NVF_{81}–GMA_{14}–NVE_5) and NVE-free (H-NVF_{66}–GMA_{34}) microgels a weak (but noticeable) band at 1565 cm^{-1} is evident. This band is due to RNH_2 [14]. The pronounced broadening in this region for the other two systems which contain NVE and GMA (H-NVF_{73}–GMA_{22}–NVE_5 and H-NVF_{63}–GMA_{32}–NVE_5) is attributed to copolymerisation, enhanced by NVE, which forced the subsequent VAM groups to be located in a range of local environments. We conclude that for all systems VAM was produced by hydrolysis.

For all the H-NVF_x–GMA_y–NVE_z microgels as well as H-NVF_{66}–GMA_{34}, hydrolysis caused complete removal of the epoxide band at 907 cm^{-1} (Fig. S1). It follows that the GMA segments within the H-NVF_x–GMA_y–NVE_z microgels were fully accessible to aqueous OH^-. This accessibility to aqueous OH^- implies the epoxide groups resided in a shell region of the NVF_x–GMA_y–NVE_z microgels. Microgels containing epoxide groups that are accessible to aqueous phase reactions are potentially useful because epoxides are a versatile chemical handle for functionalization [25].

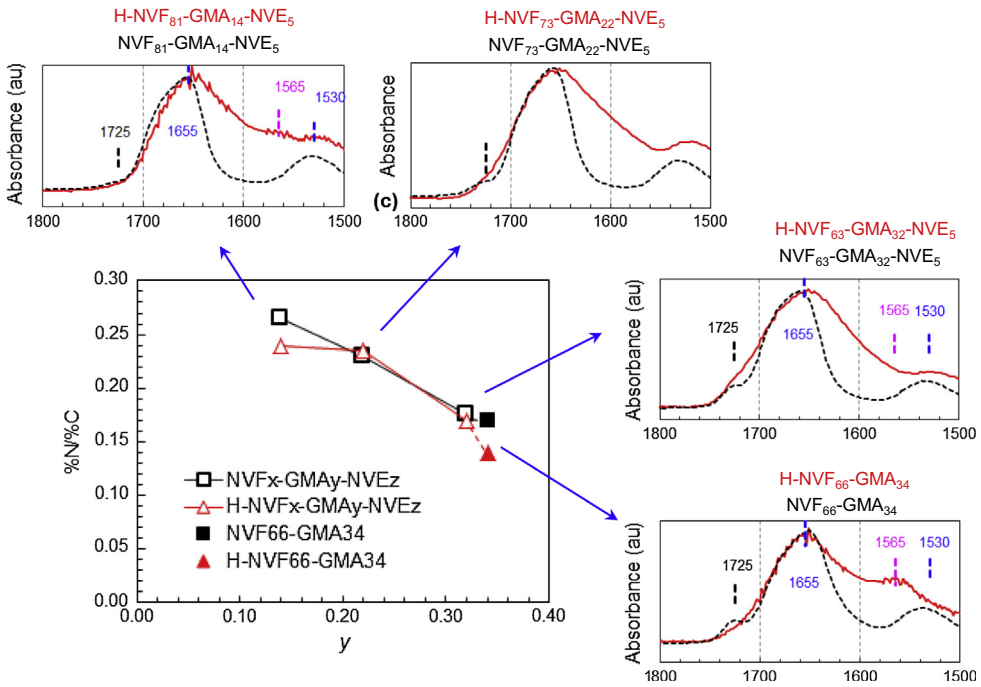

Fig. 1. Compositional changes for NVF_x–GMA_y–NVE_z particles due to hydrolysis. The graph shows the variation of the measured %N/%C ratio as a function of *y*. FTIR spectra corresponding to the data points are shown. The dotted and solid lines are for non-hydrolysed and hydrolysed systems, respectively. The error bars for the %/N/%C data points were smaller than the data point symbols.

3.2. Microgel particle morphologies swelling and effect of NVE

The non-hydrolysed NVF_x–GMA_y–NVE_z particles were colloidally stable as-made and existed as isolated latex particles in ethanol (Fig. 2(a), (d) and (g)). The dispersions were also colloidally stable when dispersed in water in microgel form and were presumably sterically stabilized (Fig. 2(b), (e) and (h)). The assumption of steric stabilisation was supported by low ζ values (less than 5 mV, Fig. 5(a)). The H-NVF_{63}–GMA_{32}–NVE_5 microgels did not show pronounced swelling visually (Fig. 2(c), (f) and (i)). However, the H-NVF_{66}–GMA_{34} particles (Fig. 2(l)) exhibited very strong swelling upon hydrolysis. The inclusion of 5 mol.% NVE within the H-NVF_x–GMA_y–NVE_z strongly restricted swelling upon hydrolysis. This was expected because NVE is not cleaved by alkaline hydrolysis [14,21], unlike other crosslinking monomers used elsewhere to prepare PVAM microcapsules [22].

The morphologies of NVF_x–GMA_y–NVE_z systems before and after hydrolysis were examined using SEM (Fig. 3). (Lower magnification images appear in Fig. S2.) The non-hydrolysed NVF_x–GMA_y–NVE_z latex particles (Fig. 3(a), (d) and (g)) were mostly featureless. (The buckling apparent is discussed below.) Importantly, they did not show the cane-ball morphology that was present for NVF_{66}–NVE_{34} (Fig. 3(j)). This difference between mostly featureless (H-)NVF_x–GMA_y–NVE_z microgels and cane-ball morphologies for (H-)NVF_{66}–GMA_{34} persisted through to the non-hydrolysed microgel particles (Fig. 3, second row) and also the hydrolysed microgels (Fig. 3, bottom row). The inclusion of NVE prevented formation of the cane-ball morphology for (H-)NVF_x–GMA_y–NVE_z latexes and microgels. The cane-ball morphology was reported earlier [15] for related NVF–GMA particles and was ascribed to microphase separation of NVF- and GMA-rich regions at the particle surface. The PGMA and PNVF phases are not compatible and the GMA-rich phase is proposed to precipitate later during particle formation; whereas, the NVF-rich phase was mostly formed in the early stages. The incompatibility between the phases is proposed to favour formation on GMA-rich phases on regions which were already GMA-rich and this process resulted in GMA-rich ridges on the particle surface. The final morphology resembles a cane-ball. It must be noted that shrinkage during SEM sample preparation and viewing could also have contributed to the cane-ball morphology. The ability of NVE to prevent the cane-ball morphology is a new observation and implies that NVE incorporated into the NVF_x–GMA_y–NVE_z particles kinetically trapped a more uniform distribution of NVF and GMA segments at the surface before polymer incompatibility between poly(NVF) and poly(GMA) segments could cause microphase separation.

The (H-)NVF_x–GMA_y–NVE_z microgels (Fig. 3, middle and bottom rows) showed a deformed, buckled, morphology which is a new morphology for NVF microgels. Evidence is presented from DLS measurements in the following that the (H-)NVF_x–GMA_y–NVE_z microgel particles were substantially swollen in water. Accordingly, these buckled morphologies are what one would expect from core–shell microgels that were swollen prior to deposition on an SEM stub. This observed buckling is most likely related to the stabilising capability of the shell under the high vacuum conditions used for SEM investigation.

The values of number-average diameters (D_{SEM}) were measured from SEM images and are shown in Fig. 4(a). (The size distributions are shown in Fig. S3.) For NVF_x–GMA_y–NVE_z particles in latex form deposited (open squares) the D_{SEM} values were all close to 1.0 μm. The initial particle inception for NAD involves nuclei formation [31]. The fact that the values for the non-hydrolysed latexes were similar suggests that NVE did not significantly affect particle nucleation and growth. This result is different to that often reported for conventional NAD polymerisation systems where inclusion of low levels of crosslinking monomer (e.g., 0.6 wt.% of divinylbenzene) can have a major effect on particle size and polydispersity [32]. It can be seen from Fig. 4(a) that there was a general, modest, increase for most of the D_{SEM} values after each latex was redispersed in water to give non-hydrolysed microgel (circles) and subsequently hydrolysed (triangles). This increase was most pronounced for the model system (y = 0.34, (H-)NVF_{66}–GMA_{34}) where the large

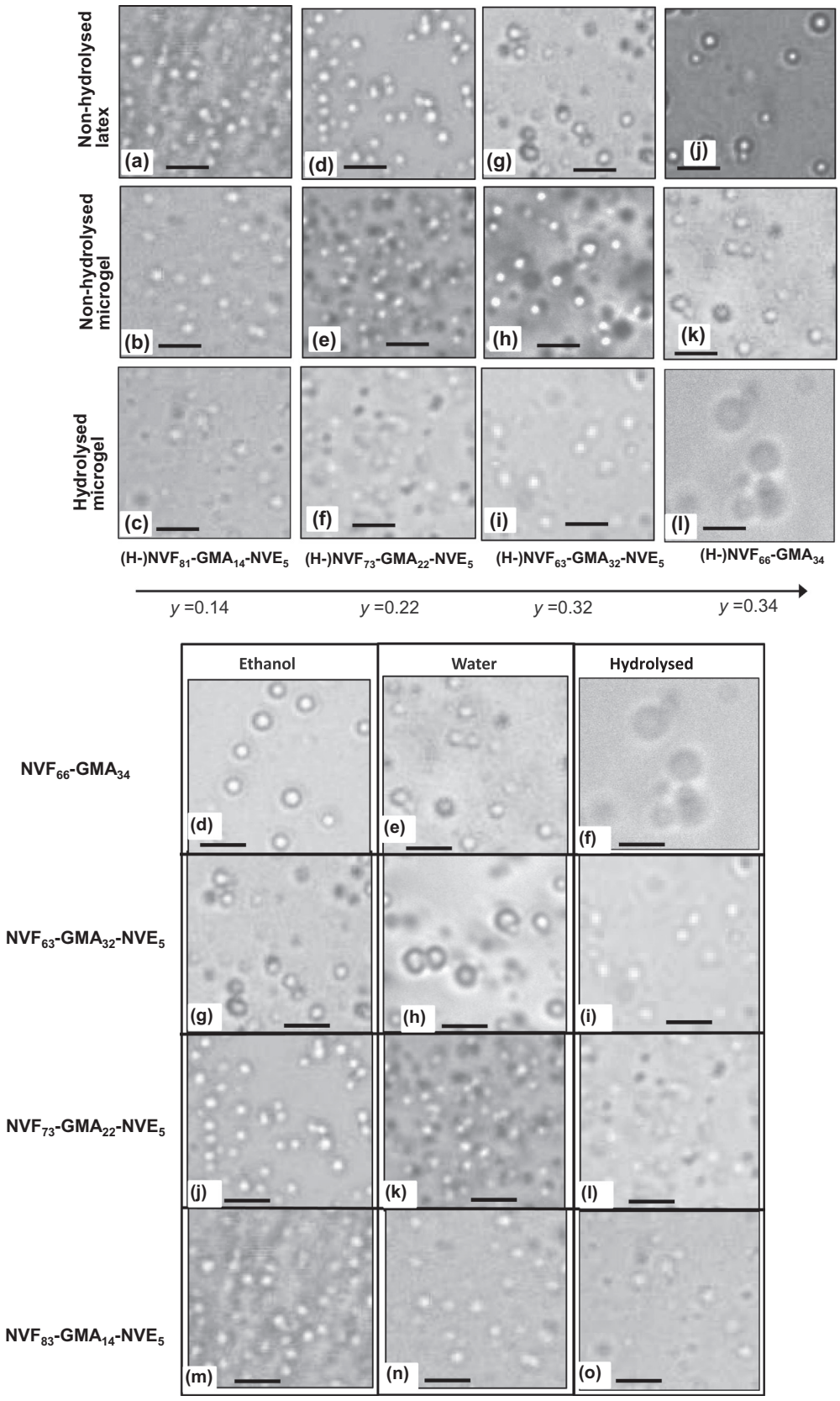

Fig. 2. Optical micrographs for various dispersions. The identities of the systems are shown below each column. The hydrolysed particles are shown in the bottom row. The scale bars are 5 μm.

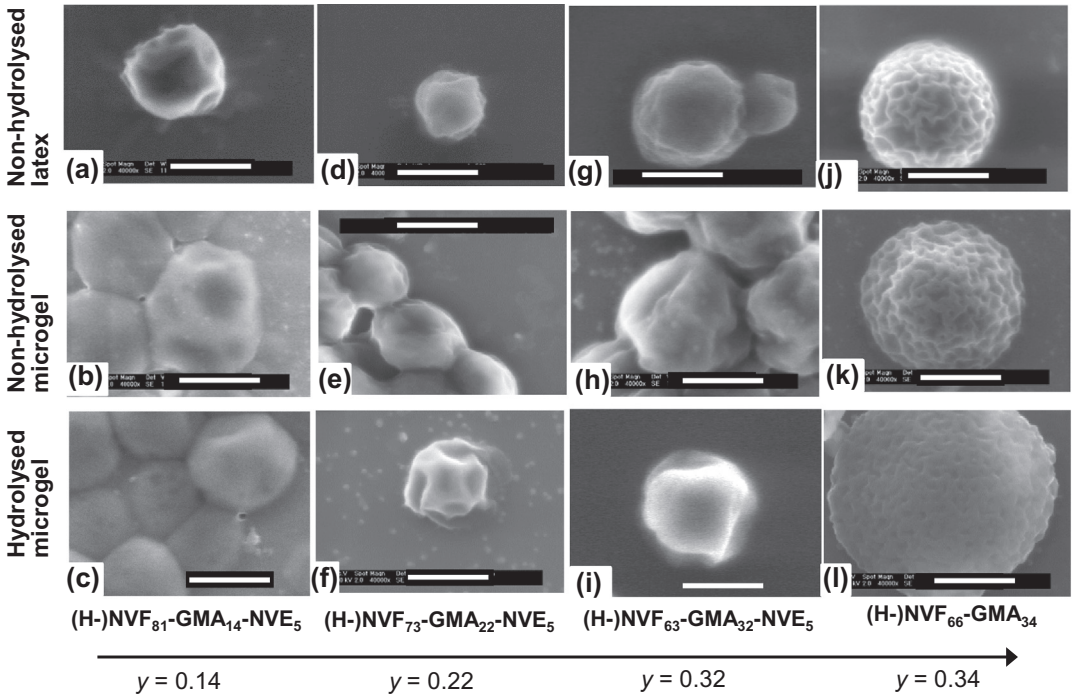

Fig. 3. SEM images for various latexes and microgels. The identities of the systems are shown below each column. The hydrolysed particles are shown in the bottom row. The scale bars are 1 μm.

D_{SEM} value was due to pronounced irreversible swelling. This result demonstrates the strong effect NVE inclusion had on providing significant stability to particle swelling.

The hydrodynamic diameters (d_h) of the latexes and microgels were measured using DLS (Fig. 4(b)). The d_h values for the NVF_x–GMA_y–NVE_z latex particles were similar to the D_{SEM} values for those particles (Fig. 4(a)), confirming good dispersion stability in ethanol. For the latex and microgel form of the NVF_x–GMA_y–NVE_z particles it can be seen that d_h increased upon redispersion of the particles in water. This demonstrates that the NVF_x–GMA_y–

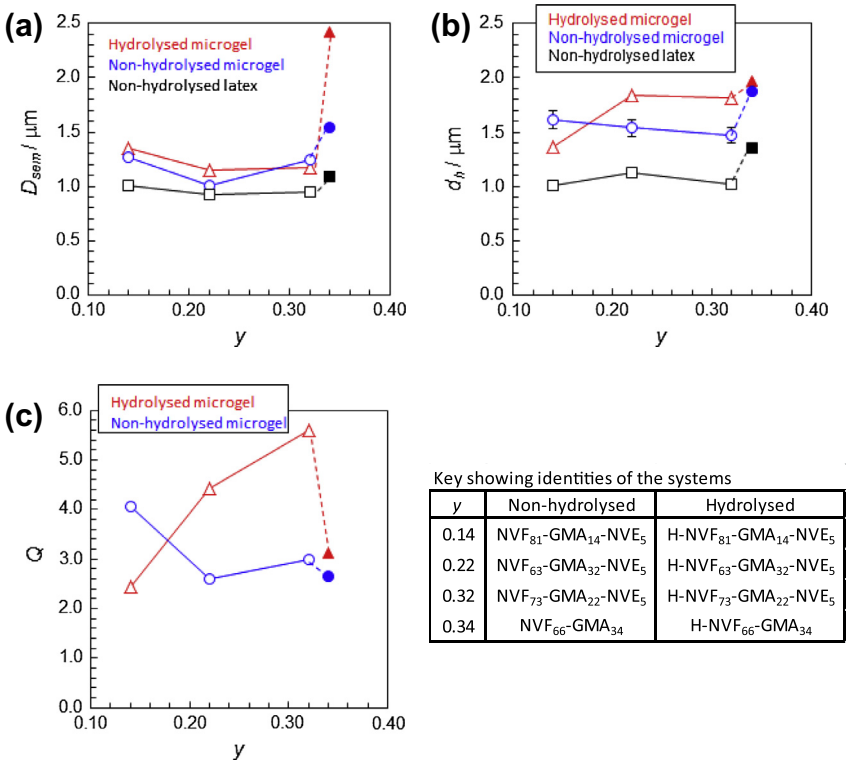

Key showing identities of the systems

y	Non-hydrolysed	Hydrolysed
0.14	NVF_{81}-GMA_{14}-NVE_5	H-NVF_{81}-GMA_{14}-NVE_5
0.22	NVF_{63}-GMA_{32}-NVE_5	H-NVF_{63}-GMA_{32}-NVE_5
0.32	NVF_{73}-GMA_{22}-NVE_5	H-NVF_{73}-GMA_{22}-NVE_5
0.34	NVF_{66}-GMA_{34}	H-NVF_{66}-GMA_{34}

Fig. 4. Particle size, swelling and composition. (a) Shows number-average diameters from SEM plotted as a function of the GMA mole fraction (y). (b) Shows the variation of the hydrodynamic diameters with y. (c) Shows the variation of the particle volume swelling ratio with y. The identities for y are shown in the table.

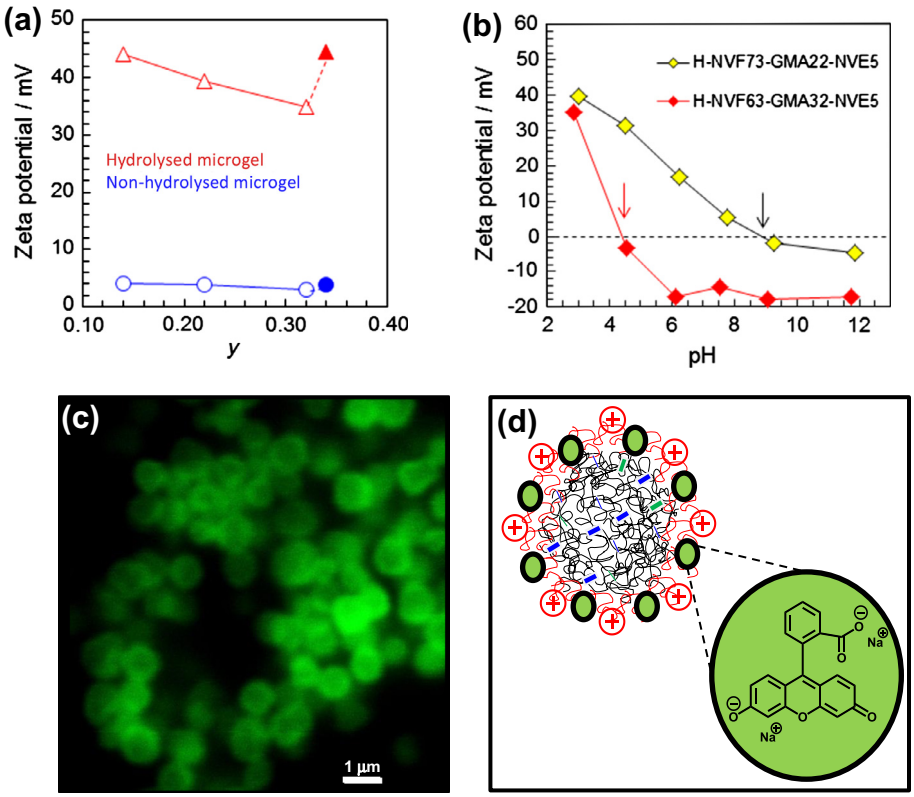

Fig. 5. Electrokinetic properties and core–shell morphology for hydrolysed microgels. (a) And (b) show the variation of the zeta potential with composition or pH for various microgel dispersions. The data for (a) were measured at pH = 3. The arrows in (b) indicate the isoelectric points. (c) Shows a confocal microscopy image of H-NVF$_{73}$–GMA$_{22}$–NVE$_5$ microgel particles labelled with sodium fluorescein and dispersed in water with a pH of 5.8. (d) Shows the structure of sodium fluorescein and depicts its proposed binding site within the shell of core–shell microgel particles.

NVE$_z$ particles were swollen by water and were, in fact, microgels. There is some evidence of a linear decrease for the d_h values for the non-hydrolysed microgels in water (open circles in Fig. 4(b)), which would indicate that swelling decreases with increasing GMA content (as expected). Interestingly, the hydrolysed microgels showed a different trend. The H-NVF$_{81}$–GMA$_{14}$–NVE$_5$ microgel (y = 0.14) had the smallest d_h values for all of the hydrolysed systems, which is evidence of fragmentation. This system was the least crosslinked of all the H-NVF$_x$–GMA$_y$–NVE$_z$ systems studied.

To gain further insight values for the particle volume swelling ratio, Q, was determined from DLS measurements by assuming (Fig. 4(c)) in pH = 3 water. These data show that Q increases and passes through a maximum for y = 0.32. This is at first glance counter-intuitive because an increase in y (GMA content) should render the hydrolysed particles more hydrophobic and they should swell less. However, we propose that the y = 0.32 system exhibited the least hydrolysis-induced fragmentation because it contained NVE and the highest GMA content. Both of these acted as crosslinkers and reduced the amount of fragmentation. (Fragmentation of microgels is known to give artificially low Q values [1].) Accordingly, fragmentation was most pronounced for the extreme composition systems with y = 0.14 and 0.34 (no NVE). This is in agreement with the interpretation of the composition data from Fig. 1 (above).

Additional evidence that PVAM was produced by hydrolysis was obtained from zeta potential data. Fig. 5(a) shows a major increase of ζ with hydrolysis implying VAM production at the microgel surface occurred. Fig. 5(a) shows that the ζ value decreased linearly with increasing y for the H-NVF$_x$–GMA$_y$–NVE$_z$ microgels. This is what would be expected for VAM groups diluted with (hydrolysed) GMA segments and strongly suggests that the surface of the H-NVF$_x$–GMA$_y$–NVE$_z$ microgels contained regions of PVAM and hydrolysed PGMA segments. These data strongly suggest that a copolymer of VAM and H-GMA was present at the surface of the H-NVF$_x$–GMA$_y$–NVE$_z$ microgels, providing evidence for core–shell PVAM microgels. The ζ value was relatively high for H-NVF$_{66}$–NVE$_{34}$ and this may be due to a higher surface concentration of PVAM species as a consequence of pronounced microphase separation and fragmentation.

The variation of ζ with pH was also investigated (Fig. 5(b)). The hydrolysed microgels were cationic at low pH and anionic at higher pH values. This is evidence of polyampholyte microgel behaviour [33]. The pK_a of PVAM is about [34] 10. The isoelectric points for H-NVF$_{63}$–GMA$_{32}$–NVE$_5$ and H-NVF$_{73}$–GMA$_{22}$–NVE$_5$ were approximately 4.5 and 9.0, respectively. It follows that there were anionic groups present which contributed to the negative ζ values at high pH. A likely candidate for these groups is RCOO$^-$ from hydrolysis of GMA units. Our earlier study on H-NVF–GMA microgels also identified polyampholyte behaviour [15]. However, those systems exhibited large scale fragmentation and the shells detached as a result of hydrolysis. The present systems were far more robust as a consequence of NVE inclusion, which is an important advantage afforded by NVE.

We employed confocal microscopy to probe the location of the amine groups within the hydrolysed microgels. The *anionic* fluorescent probe (sodium fluorescein) was added to *cationic* H-NVF$_{73}$–GMA$_{22}$–NVE$_5$ microgel particles at pH = 5.8 and allowed to equilibrate and then washed extensively. A representative confocal microscopy image shown in Fig. 5(c) which shows the particles had a green[1] shell and dark core. The image confirms the presence of a cationic (amine-rich) shell. The relatively dark cores implies that

[1] For interpretation of color in Fig. 5, the reader is referred to the web version of this article.

the microgel particle cores were deficient of VAM-segments and is consistent with a non-hydrolysed NVF-rich core. The proposed binding sites of the fluorophore is depicted in Fig. 5(d).

3.3. Microgel morphology, hydrolysis and the influence of NVE crosslinker

Based on the data presented above we propose the general structures for the NVF_x–GMA_y–NVE_z latexes and microgels shown in Scheme 1. We interpret the SEM images obtained for the non-hydrolysed latex particles and microgels (Fig. 3) in terms of core–shell NVF_x–GMA_y–NVE_z latexes and microgels, respectively, with a water-swellable NVF-rich core and NVF–GMA-rich shell. Incorporation of NVE prevented phase separation of NVF and GMA in the shell. It also prevented large scale irreversible swelling and major shell fragmentation during hydrolysis. A more uniform shell was produced due to copolymerisation between the NVF and GMA monomers in the presence of NVE. The shell is proposed to have contained two types of crosslinking; conventional NVE-crosslinking and also NVF–GMA crosslinking [15]. Hydrolysis had a major effect on the periphery of the particles. The shell of the microgels contained VAM and hydrolysed GMA. The latter contained negatively charged fragments. These charged species were both present in the shell (as depicted in Scheme 1) and polyampholyte microgels resulted. Support for the negative charges originating from hydrolysed GMA segments came from the fact that ζ values for PGMA particles hydrolysed in the same manner were about − 10 mV across the same pH range as shown in Fig. 5(b). The core of the microgels was NVF-rich. A beneficial role of NVE that was apparent in this work was its ability to stabilize the polyampholyte structure against large scale fragmentation.

An intriguing question that has arisen from this work concerns why the hydrolysis of all the H-NVF_x–GMA_y–NVE_z microgels were not complete. The conditions used were suitable for fully hydrolysing NVF–NVE based on previous work [15] and was also verified using a NVF–NVE microgel (data not shown). The ratio of OH^- groups to amide units was about 14:1, which is well above the critical value of 1:1 identified for alkaline hydrolysis of linear poly(NVF) [16]. However, the key difference is that negatively charged groups were generated by hydrolysis of the GMA units within the H-NVF_x–GMA_y–NVE_z microgels. Those groups would have provided local electrostatic repulsion for the incoming OH^- groups, thereby decreasing the extent of hydrolysis, particularly in the core of the microgels. This is consistent with the equivalent reported observation that acid hydrolysis of linear poly(NVF) to poly(VAM) is relatively inefficient because of electrostatic repulsion between protons and RNH_3^+ groups [16].

We note that the new water-swellable core–shell microgels studied here have potential for application in areas such as hybrid particles (amine groups), biomaterials (amine and epoxide functionality) and surfaced coatings. Of course the cytocompatibility of primary amines may need optimisation; however, several approaches have been successfully established for related polymers [35,36] for this purpose which may be suitable for use with PVAM based microgels.

4. Conclusions

We have synthesised and investigated the morphologies and properties two new families of water-swellable core–shell microgels; NVF_x–GMA_y–NVE_z and H-NVF_x–GMA_y–NVE_z. NVE forced a uniform distribution of the NVF and GMA segments in the particle shell as judged by the absence of the cane-ball morphology from SEM. Interestingly, upon alkali treatment the NVF groups in the core of the GMA-containing microgels were not hydrolysed. The GMA-rich shell appears to have indirectly decreased the core reactivity and this was attributed to an electrostatic mechanism. This is potentially beneficial from the perspective of designing water-swellable core–shell microgels with a functionalised shell. Primary amine groups are well suited to functionalization reactions [17]. The H-NVF_x–GMA_y–NVE_z microgels were polyampholyte-like and were stabilized to a considerable extent by NVE. The NVF_x–GMA_y–NVE_z and H-NVF_x–GMA_y–NVE_z microgels had, respectively, accessible epoxide and primary amine groups. It was demonstrated that all of the epoxide groups (from GMA) were available for hydrolysis.

Acknowledgment

BRS and RVU would like to thank the EPSRC for funding.

Appendix A. Supplementary material

Supplementary data associated with this article can be found, in the online version, at http://dx.doi.org/10.1016/j.jcis.2013.09.030.

References

[1] B.R. Saunders, N. Laajam, E. Daly, S. Teow, X. Hu, R. Stepto, Adv. Colloid Interface Sci. 147–148 (2009) 251.
[2] J.C. Gaulding, M.H. Smith, J.S. Hyatt, A. Fernandez-Nieves, L.A. Lyon, Macromolecules 45 (2012) 39.
[3] V. Castro-Lopez, J. Hadgraft, M.J. Snowden, Int. J. Pharm. 292 (2005) 137.
[4] T. Hoare, R. Pelton, Curr. Opin. Colloid Interface Sci. 13 (2008) 413.
[5] L. Hu, M.J. Serpe, J. Mater. Chem. 22 (2012) 8199.
[6] R. Mansson, H. Bysell, P. Hansson, A. Schmidtchen, M. Malmsten, Biomacromolecules 12 (2011) 419.
[7] W. Richtering, Langmuir 28 (2012) 17218.
[8] I. Berndt, W. Richtering, Macromolecules 36 (2003) 8780.
[9] C.D. Jones, L.A. Lyon, Macromolecules 36 (2003) 1988.
[10] D. Gan, L.A. Lyon, Prog. Colloid Polym. Sci. 133 (2006) 1.
[11] B.E. Rodriguez, M.S. Wolfe, M. Fryd, Macromolecules 27 (1994) 6642.
[12] S. Lally, F. Cellesi, T. Freemont, B.R. Saunders, Colloid Polym. Sci. 289 (2011) 647.
[13] D. Dupin, S. Fujii, S.P. Armes, P. Reeve, S.M. Baxter, Langmuir 22 (2006) 3381.
[14] S. Thaiboonrod, C. Berkland, A.H. Milani, R. Ulijn, B.R. Saunders, Soft Matter 9 (2013) 3920.
[15] S. Thaiboonrod, F. Cellesi, R.V. Ulijn, B.R. Saunders, Langmuir 28 (2012) 5227.
[16] L. Gu, S. Zhu, A.N. Hrymak, J. Appl. Polym. Sci. 86 (2002) 3412.
[17] R.K. Pinschmidt, J. Polym. Sci. A Polym. Chem. 48 (2010) 2257.
[18] J. Xu, R. Pelton, J. Colloid Interface Sci. 276 (2004) 113.
[19] C. Miao, X. Chen, R. Pelton, Ind. Eng. Chem. Res. 46 (2007) 6486.
[20] J. Xu, A.B. Timmons, R. Pelton, Colloid Polym. Sci. 282 (2004) 256.
[21] Z. Mohammadi, A. Cole, C. Berkland, J. Phys. Chem. C 113 (2009) 7652.
[22] J. Kim, H.-J. Lim, Y.K. Hwang, H. Woo, J.W. Kim, K. Char, Langmuir 28 (2012) 11899.
[23] L. Shi, C. Berkland, Macromolecules 40 (2007) 4635.
[24] T.C. Suekama, V. Aziz, Z. Mohammadi, C. Berkland, S.H. Gehrke, J. Polym. Sci. (A) Polym. Chem. 51 (2013) 435.
[25] A. Gloria, F. Causa, T. Russo, E. Battista, R.D. Moglie, S. Zeppetelli, R. De Santis, P.A. Netti, L. Ambrosio, Biomacromolecules 13 (2012) 3510.
[26] R. Liu, A.H. Milani, T.J. Freemont, B.R. Saunders, Soft Matter 7 (2011) 4696.
[27] K. Ishii, Colloid Surf. A 153 (1999) 591.
[28] R. Contreras-Caceres, A. Sanchez-Iglesias, M. Karg, I. Pastoriza-Santos, J. Perez-Juste, J. Pacifico, T. Hellweg, A. Fernandez-Barbero, L.M. Liz-Marzan, Adv. Mater. 20 (2008) 1666.
[29] D.J. Shaw, Introduction to Colloid and Surface Chemistry, Butterworth-Heinemann, Oxford, 1993.
[30] Y. Maeda, T. Higuchi, I. Ikeda, Langmuir 16 (2000) 7503.
[31] L. Antl, J.W. Goodwin, R.D. Hill, R.H. Ottewill, S.M. Owens, S. Papworth, J.A. Waters, Colloid Surf. 17 (1986) 67.
[32] C.M. Tseng, Y.Y. Lu, M.S. El-Asser, J.W. Vanderhoff, J. Polym. Sci. A Polym. Chem. 24 (1986) 2995.
[33] B.S. Ho, B.H. Tan, J.P.K. Tan, K.C. Tam, Langmuir 24 (2008) 7698.
[34] K. Samaru, H. Matsuoka, H. Yamaoka, J. Phys. Chem. 100 (1996) 9000.
[35] H. Cai, X. An, J. Cui, J. Li, S. Wen, K. Li, M. Shen, L. Zheng, G. Zhang, X. Shi, ACS Appl. Mater. Interfaces 5 (2013) 1722.
[36] W.Y. Seow, K. Liang, M. Kurisawa, C.A.E. Hauser, Biomacromolecules 14 (2013) 2340.